

Microscopic Optical Potential Description of Elastic Scattering and Breakup Reactions of Light Exotic Nuclei

V. K. Lukyanov¹, E. V. Zemlyanaya¹, K. V. Lukyanov¹, A. N. Antonov²,
D. N. Kadrev², M. K. Gaidarov², K. Spasova^{2,3}

¹Joint Institute for Nuclear Research, Dubna 141980, Russia

²Institute for Nuclear Research and Nuclear Energy, Bulgarian Academy of Sciences, Sofia 1784, Bulgaria

³Ep. K. Preslavski University of Shumen, 9712 Shumen, Bulgaria

Abstract. The hybrid model of the microscopic optical potential (OP) is applied to calculate the $^{11}\text{Li}+p$, $^{10,11}\text{Be}+p$ and $^{10,11}\text{Be}+^{12}\text{C}$, $^8\text{B}+^{12}\text{C}$, $^8\text{B}+^{58}\text{Ni}$, and $^8\text{B}+^{208}\text{Pb}$ elastic scattering cross sections at energies $E < 100$ MeV/nucleon. Previously, we have performed studies of elastic scattering of ^6He and ^8He isotopes on protons and ^{12}C target. The OPs contain the folding-model real part with the direct and exchange isoscalar and isovector terms included, while its imaginary part is derived within an approach to the high-energy approximation (HEA). The depths of the real and imaginary parts of OP (ReOP and ImOP) are fitted to the elastic scattering data, being simultaneously adjusted to reproduce the true energy dependence of the corresponding volume integrals. In the calculations, microscopic density distributions of exotic projectiles were used, such as large-scale shell model (LSSM) densities of ^{11}Li , densities of ^{10}Be and ^8B nuclei obtained within the quantum Monte Carlo model, generator coordinate method densities of $^{10,11}\text{Be}$, and three-cluster model densities of ^8B . Also, the cluster models, in which ^{11}Li consists of $2n$ -halo and the ^9Li core having its own LSSM form of density and ^{11}Be consists of a n -halo and the ^{10}Be core, are adopted. Within the latter, we give predictions for the longitudinal momentum distributions of ^9Li fragments produced in the breakup of ^{11}Li at 62 MeV/nucleon on a proton target. It is shown that our results for the diffraction and stripping reaction cross sections in ^{11}Be scattering on ^9Be , ^{93}Nb , ^{181}Ta , and ^{238}U targets at 63 MeV/nucleon are in a good agreement with the available experimental data. It is shown, in general, that this microscopic approach can be successfully applied to studies of exotic nuclei with a pronounced neutron- or proton-halo structure.

1 Introduction

The experiments with intensive secondary radioactive nuclear beams have made it possible to investigate the structure of light nuclei near the neutron and proton drip lines as well as the mechanism of scattering of the weakly bound nuclei [1, 2]. A special attention has been paid to the neutron-rich isotopes of helium (${}^6,8\text{He}$), lithium (${}^{11}\text{Li}$), beryllium (${}^{14}\text{Be}$) and others, in which several neutrons are situated in the far extended nuclear periphery and form a "halo". A widely used way to study the structure of exotic nuclei is to analyze their elastic scattering on protons and nuclear targets at different energies. Elastic scattering measurements at low energies (near to or above the Coulomb barrier) have been used as an effective tool to investigate the unusual features of exotic nuclei, such as extended halos or neutron skins. The exotic structure of these light nuclei changes the elastic scattering due to competing mechanisms such as breakup and transfer reactions.

In this work (see also [3, 4], as well as in our previous works considering processes with exotic He isotopes [5–7]), we use microscopically calculated OPs within the hybrid model [8, 9]. In the latter the ReOP is calculated by a folding of a nuclear density and the effective nucleon-nucleon (NN) potentials [10] and includes both direct and exchange parts. The ImOP is obtained within the HEA model [11, 12]. There are only two or three fitting parameters in the hybrid model that are related to the depths of the ReOP, ImOP and the spin-orbit (SO) part of the OP. For the ${}^{11}\text{Li}+p$ elastic scattering we have used the realistic microscopic LSSM [13, 14] density of ${}^{11}\text{Li}$, while the density distributions of ${}^{10,11}\text{Be}$ nuclei obtained within the quantum Monte Carlo (QMC) model [15] and the generator coordinate method (GCM) [16] are used to calculate the microscopic OPs and cross sections of elastic scattering of these nuclei on protons and ${}^{12}\text{C}$. For the case of elastic scattering of ${}^8\text{B}$ on different nuclei the variational Monte Carlo (VMC) [17] and three-cluster model (3CM) [18] densities of ${}^8\text{B}$ are applied.

The main goal of our work is to calculate the differential cross sections of elastic ${}^{11}\text{Li}$, ${}^{10,11}\text{Be}$, and ${}^8\text{B}$ scattering on protons and nuclei at energies less than 100 MeV/nucleon studying the possibility to describe the existing experimental data by calculating microscopically not only the ReOP, but also the ImOP (instead of using phenomenological one) within the HEA and using a minimal number of fitting parameters. Also, we estimate other characteristics of the reaction mechanism such as the total reaction and breakup cross sections and momentum distributions of the cluster fragments.

2 Elastic Scattering of ^{11}Li , $^{10,11}\text{Be}$, and ^8B on Protons and Nuclei at Energies $E < 100$ MeV/nucleon

2.1 Hybrid model of the microscopic optical potential

The microscopic OP that contains the volume real (V^F) and imaginary parts (W), and the spin-orbit interaction (V^{ls}) is used for calculations of elastic scattering differential cross sections. We introduce a set of weighting coefficients N_R , N_I , N_R^{ls} and N_I^{ls} that are related to the depths of the corresponding parts of the OP and are obtained by a fitting procedure to the available experimental data. The OP has the form:

$$U(r) = N_R V^F(r) + i N_I W(r) - 2\lambda_\pi^2 \times \left[N_R^{ls} V_R^{ls} \frac{1}{r} \frac{df_R(r)}{dr} + i N_I^{ls} W_I^{ls} \frac{1}{r} \frac{df_I(r)}{dr} \right] (\vec{l} \cdot \vec{s}), \quad (1)$$

where $2\lambda_\pi^2 = 4 \text{ fm}^2$ with the squared pion Compton wave length $\lambda_\pi^2 = 2 \text{ fm}^2$. Let us denote the values of the ReOP and ImOP at $r = 0$ by $V_R(\equiv V^F(r = 0))$ and $W_I(\equiv W(r = 0))$. We note that the spin-orbit part of the OP contains real and imaginary terms with the parameters V_R^{ls} and W_I^{ls} related to V_R and W_I by the $V_R^{ls} = V_R/4$ and $W_I^{ls} = W_I/4$, correspondingly. Here V_R and W_I (and V_R^{ls} and W_I^{ls}) have to be negative.

The ReOP $V^F(r)$ of the nucleon-nucleus OP is assumed to be a result of the folding of the nuclear density with an effective NN potential and is a sum of isoscalar (V_{IS}^F) and isovector (V_{IV}^F) components. Each of them has its direct (V_{IS}^D and V_{IV}^D) and exchanged (V_{IS}^{EX} and V_{IV}^{EX}) parts. The effective NN potential contains an energy dependence usually taken in the form $g(E) = 1 - 0.003E$ and a density dependence with the form for the CDM3Y6 effective Paris potential [10]

$$F(\rho) = C \left[1 + \alpha e^{-\beta\rho(r)} - \gamma\rho(r) \right] \quad (2)$$

with $C=0.2658$, $\alpha=3.8033$, $\beta=1.4099 \text{ fm}^3$, and $\gamma=4.0 \text{ fm}^3$. They have their isoscalar and isovector components in the form of M3Y interaction obtained within g -matrix calculations using the Paris NN potential [10,19].

The ImOP can be chosen either to be in the form of the microscopically calculated V^F ($W = V^F$) or in the form W^H obtained in Refs. [8,9] within the HEA of the scattering theory:

$$W^H(r) = -\frac{\bar{\sigma}_N}{2\pi^2} \frac{E}{k} \int_0^\infty j_0(kr) \rho_p(q) \rho_t(q) f_N(q) q^2 dq. \quad (3)$$

In Eq. (3) $\rho(q)$ are the corresponding formfactors of the nuclear densities, $f_N(q)$ is the amplitude of the NN scattering and $\bar{\sigma}_N$ is the averaged over

the isospin of the nucleus total NN scattering cross section that depends on the energy. The parametrization of the latter dependence can be seen, e.g., in Ref. [5]. We note that to obtain the HEA OP (with its imaginary part W^H in Eq. (3)) one can use the definition of the eikonal phase as an integral of the nucleon-nucleus potential over the trajectory of the straight-line propagation and has to compare it with the corresponding Glauber expression for the phase in the optical limit approximation.

In the spin-orbit parts of the OP the functions $f_i(r)$ ($i = R, I$) correspond to Woods-Saxon (WS) forms of the potentials with parameters of the real and imaginary parts V_R, W_I, R_i, a_i [$f_R(r, R_R, a_R)$ and $f_I(r, R_I, a_I)$], as they are used in the DWUCK4 code [20] and applied for numerical calculations. We determine the values of these parameters by fitting the WS potentials to the microscopically calculated potentials $V^F(r)$ and $W(r)$.

2.2 Results of calculations of elastic scattering cross sections

We consider $^{11}\text{Li}+p$ elastic scattering at three energies, 62, 68.4, and 75 MeV/nucleon, for which the differential cross sections have been measured (see Ref. [3]). In Figure 1 we give the differential cross section of the elastic scattering $^{11}\text{Li}+p$ at 62 MeV/nucleon in the cases when $W = W^H$ and $W = V^F$ with and without accounting for the spin-orbit term in Eq. (1). The renormalization parameters N are determined by a fitting procedure. The results of the calculations are close to each other and that is why all of them are presented inside areas shown in Figure 1. The blue area includes four curves corresponding to $W = W^H$ (from which three curves obtained without SO term and one with the SO term), while the grey one includes four curves corresponding to $W = V^F$ (from which two curves obtained without SO term and two curves with the SO term). We give in Table 1 the values of the N 's parameters, χ^2 and the total reaction cross sections σ_R .

Another physical criterion that has to be imposed on the choice of the N values is the behavior of the volume integrals

$$J_V = \frac{4\pi}{A} \int dr r^2 [N_R V^F(r)], \quad (4)$$

$$J_W = \frac{4\pi}{A} \int dr r^2 [N_I W^H(r)] \quad (5)$$

as functions of the energy. It was pointed out in [22] that the volume integral J_V decreases with the increase of the energy in the interval $0 < E < 100$ MeV/nucleon, while J_W increases with the increase of comparatively small energy and becomes almost constant at a larger energy.

It is accepted that the elastic scattering of light nuclei is rather sensitive to their periphery, where transfer and breakup processes also take place.

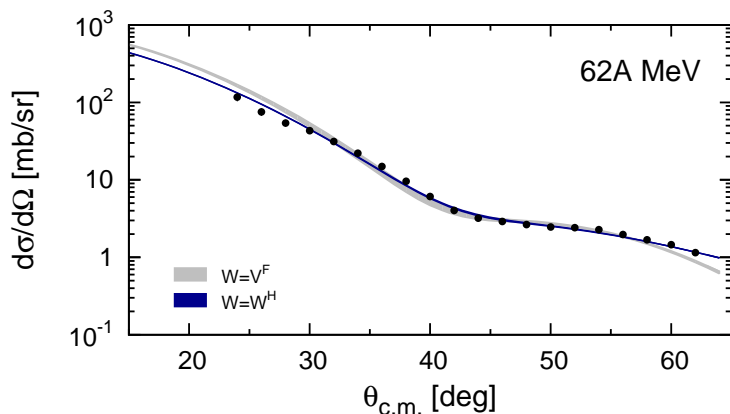


Figure 1: The $^{11}\text{Li}+p$ elastic scattering cross section at $E = 62$ MeV/nucleon using $U(r)$ [Eq. (1)] for values of the parameters shown in Table 1. Dark (blue) area: $W = W^H$, pale (grey) area: $W = V^F$. The experimental data are taken from Ref. [21].

Table 1: Values of the N s parameters, χ^2 and σ_R (in mb) in the case of $^{11}\text{Li}+p$ at 62 MeV/nucleon for the results shown in Figure 1.

W	N_R	N_I	N_R^{SO}	N_I^{SO}	χ^2	σ_R
W^H	0.871	0.953			1.415	456.97
	0.870	0.965			1.435	459.37
	0.873	0.948			1.423	455.98
	0.854	0.974	0.028	0.000	1.468	461.21
V^F	0.953	0.448			5.567	389.72
	0.956	0.398			5.726	361.02
	0.670	0.251	0.338	0.000	5.027	258.65
	0.623	0.266	0.402	0.000	5.538	270.05

Therefore, investigating the elastic scattering, one must bear in mind that virtual non-elastic contributions can also take part in the process. The contribution from a surface imaginary term to the OP [Eq. (1)] can be considered as the so-called dynamical polarization potential, which allows one to simulate the surface effects caused by the latter. In fact, the imaginary part of the SO term in our OP [see Eq. (1)] plays effectively this role. However, sometimes one needs to increase the absorption in the surface region and thus, one adds a derivative of the ImOP (surface term):

$$W^{sf}(r) = -iN_I^{sf}r \frac{dW(r)}{dr}, \quad (6)$$

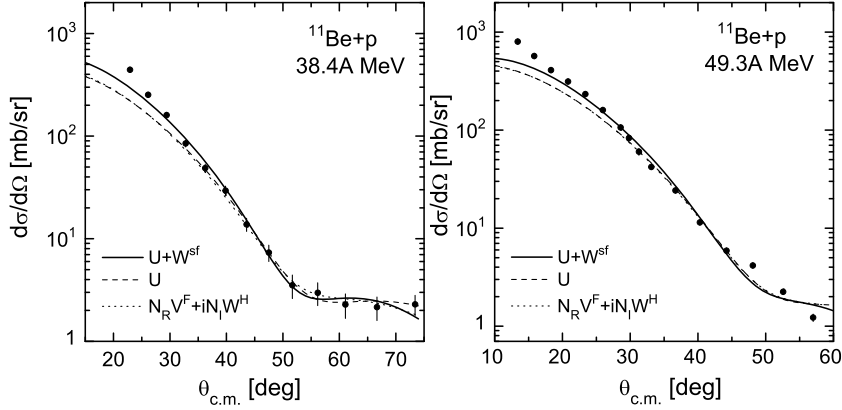


Figure 2: $^{11}\text{Be}+p$ elastic scattering cross sections. Calculations are performed with GCM density of ^{11}Be . Solid line: OP with both l_s and surface terms [Eqs. (1) and (6)]; dashed line: OP with l_s term [Eq. (1)]; dotted line: the volume part of OP from Eq. (1). Experimental data for 38.4 MeV/nucleon and 49.3 MeV/nucleon are taken from Refs. [23] and [24], respectively.

where N_I^{sf} is also a fitting parameter. Thus, we consider additionally the integral over the surface term of the OP (6):

$$J_W^{sf} = \frac{4\pi}{A} \int dr r^2 \left[N_I W^H(r) - N_I^{sf} r \frac{dW^H(r)}{dr} \right]. \quad (7)$$

In Figure 2 are given and compared with the empirical data elastic cross sections for the scattering of ^{11}Be on protons at energies 38.4 and 49.3 MeV/nucleon applying the fitting procedure for the parameters N_s . All of them are calculated using the GCM density of ^{11}Be . Various curves drawn in Figure 2 correspond to different contributions to the OP that are accounted for. One can see a discrepancy at small angles ($\theta < 30^\circ$) that seems to be related to the contributions from the surface region of interactions, where breakup processes play an important role. Similarly to the results for the $^{10}\text{Be}+p$ elastic scattering cross sections (see Figure 2 of Ref. [3]), the account for both spin-orbit and surface terms to the OP leads to a better agreement with the $^{11}\text{Be}+p$ data in the region of small angles. The corresponding values of the parameters N_R and N_I deviate from unity of about 20 – 30% that points out that the hybrid model for the OP can be used successfully in such calculations.

The calculated within the hybrid model elastic scattering cross sections of $^{11}\text{Be}+^{12}\text{C}$ (their ratios to the Rutherford one) at the same energies as for $^{10,11}\text{Be}+p$ scattering are given in Figure 3 and compared with the ex-

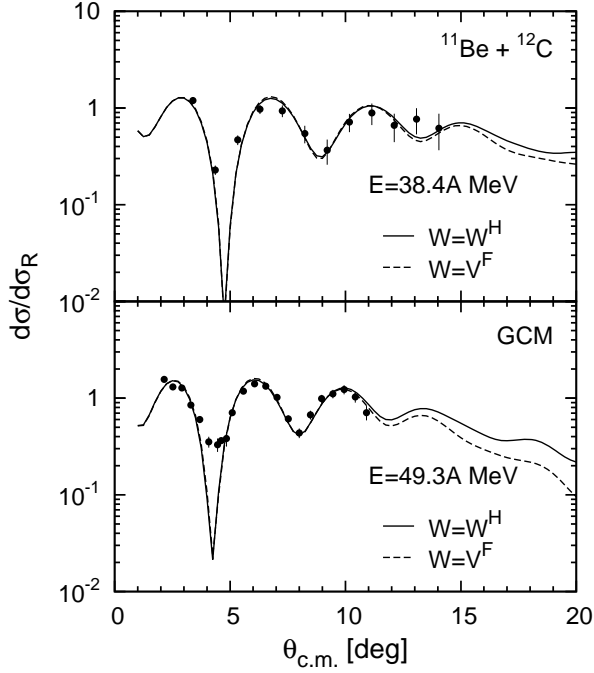


Figure 3: $^{11}\text{Be}+^{12}\text{C}$ elastic scattering cross sections. Solid lines: $W = W^H$; dashed lines: $W = V^F$. For ^{11}Be GCM density [16] was used. Experimental data for 38.4 MeV/nucleon and 49.3 MeV/nucleon are taken from Refs. [23] and [24], respectively.

perimental data. In comparison with the case of $^{10,11}\text{Be}+p$, the experimental data [23, 24] for the scattering on ^{12}C demonstrate more developed diffractive picture on the basis of the stronger influence of the Coulomb field. It can be seen in Figure 3 that in both cases of calculations of OPs with QMC or GCM densities the results are in a good agreement with the available data. It is seen also from the figure that it is difficult to determine the advantage of the use for the ImOP $W = W^H$ or $W = V^F$, because the differences between the theoretical results start at angles for which the experimental data are not available.

As an example, we present in Figure 4 our results for $^8\text{B}+^{58}\text{Ni}$ elastic scattering cross sections at energy 25.3 MeV using the VMC density. In this case, the central part of the corresponding ImOP calculated in HEA turns out to be almost one order of magnitude deeper than the real part. It is clear that this behavior of the HEA ImOP is not realistic. From other side, however, it is known that the decisive region of the OP at such energies

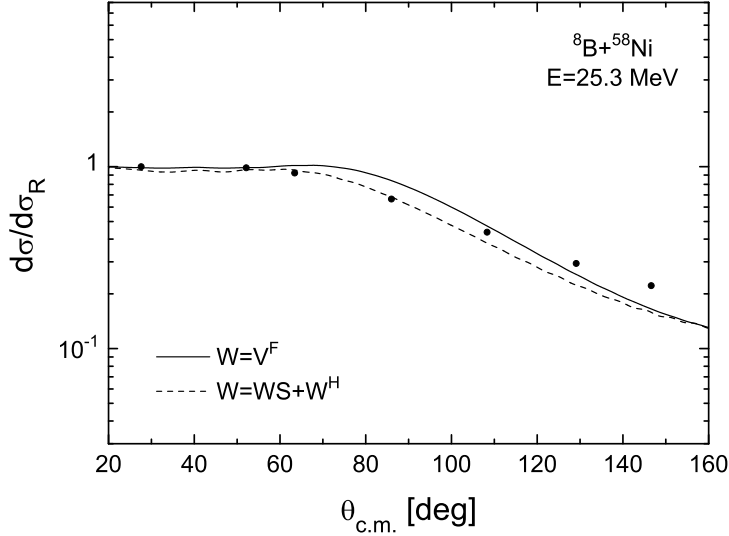


Figure 4: ${}^8\text{B}+{}^{58}\text{Ni}$ elastic scattering cross sections at $E = 25.3$ MeV calculated using the VMC density of ${}^8\text{B}$. Solid line: $W = V^F$; dashed line: $W = WS + W^H$. Experimental data are taken from Ref. [25].

close to the Coulomb barrier is the surface one. We note, as it has been pointed out in Ref. [25], that every acceptable potential has an imaginary part that is extended beyond the corresponding real part. As a result, an absorption at a large distance due to the existence of a halo state is suggested. To confirm the importance of the surface nuclear region we give two curves in Figure 4. One of them is the calculated cross section when the ImOP is taken as the folded ReOP with $N_R = N_I = 1$. The second curve corresponds to a combination of the WS single-particle potential used to analyze the data in Ref. [25] and describing the central part of OP plus the ImOP calculated within the HEA for the surface part. As it can be seen from Figure 4 both curves lead to a satisfactory description of the experimental data. A difference in the calculated results is more visible at angles larger than 60 degrees. We also obtain a result for the elastic cross section when the ImOP is calculated within the HEA, which turns out to be very similar to that obtained in the case $W = WS + W^H$ and shown in Figure 4.

3 Breakup Processes of ${}^{11}\text{Li}$ and ${}^{11}\text{Be}$ within Cluster Models

This part of the work is based on the procedure for microscopic calculations of OPs presented in Subsec. 2.1. We consider simple two-cluster models for ${}^{11}\text{Li}$ and ${}^{11}\text{Be}$ nuclei in which, first, the density distributions

of the ${}^9\text{Li}$ (${}^{10}\text{Be}$) core (c cluster) and $h = 2n$ or $h = n$ halo must be given. Second, the folding potentials of the interaction of each of the clusters with the incident proton or target nucleus have to be computed. Finally, the sum of these two potentials must be folded with the respective two-cluster density distribution of ${}^9\text{Li}$ (${}^{10}\text{Be}$), which means that the wave function of the relative motion of two clusters must be known. The latter is obtained by solving the Schrödinger equation with the Woods-Saxon potential for a particle with a reduced mass of two clusters. The parameters of the WS potentials are obtained by fitting the energy of a given state to the empirical separation energy values of the di-neutron halo $\varepsilon = 247$ KeV of ${}^{11}\text{Li}$ and the neutron halo $\varepsilon = 504$ KeV of ${}^{11}\text{Be}$, respectively, and the rms radius of the cluster function. More details how to calculate the characteristics of breakup processes of the ${}^{11}\text{Li}$ and ${}^{11}\text{Be}$ nuclei, namely diffraction and stripping reaction cross sections and the momentum distributions of the fragments, are given in Refs. [3, 4].

We perform calculations of the breakup cross sections of ${}^{11}\text{Be}$ on the target nucleus ${}^9\text{Be}$ and heavy nuclei, such as ${}^{93}\text{Nb}$, ${}^{181}\text{Ta}$, and ${}^{238}\text{U}$, and compare our results with the available experimental data [26]. The densities of these heavy nuclei needed to compute the OPs are taken from Ref. [27]. The calculated diffraction and stripping cross sections (when a neutron leaves the elastic channel) for reactions ${}^{11}\text{Be}+{}^9\text{Be}$ and ${}^{11}\text{Be}+{}^{93}\text{Nb}$, are illustrated in Figure 5. We note the good agreement with the experimental data from light and heavy breakup targets. The obtained cross sections for the diffraction and stripping have a similar shape. The values of the widths are around 50 MeV/c in agreement with the experimental ones. Our results confirm the observations (e.g., in Refs. [28, 29]) that the width almost does not depend on the mass of the target and as a result, it gives information basically about the momentum distributions of two clusters. Here we note that due to the arbitrary units of the measured cross sections of the considered processes it was not necessary to renormalize the depths of our OPs of the fragments-target nuclei interactions.

4 Conclusions

The results of the present work can be summarized as follows:

i) The optical potentials and cross sections of ${}^{11}\text{Li}+p$, ${}^{10,11}\text{Be}+p$, ${}^{10,11}\text{Be}+{}^{12}\text{C}$, ${}^8\text{B}+{}^{12}\text{C}$, ${}^8\text{B}+{}^{58}\text{Ni}$, and ${}^8\text{B}+{}^{208}\text{Pb}$ elastic scattering at energies $E < 100$ MeV/nucleon were calculated and comparison with the available experimental data was performed. The ReOP (V^F) was calculated microscopically using the folding procedure and the expression for the CDM3Y6-type of the effective interaction based on the solution of the equation for the g-matrix, in which the Paris NN potential has been used. The ImOP (W^H) was calculated within the HEA. Different micro-

scopically obtained densities of protons and neutrons in ^{11}Li , $^{10,11}\text{Be}$ and ^8B were used in the calculations: LSSM, GCM, QMC (VMC), and 3CM. The SO and surface contribution (for $^{10,11}\text{Be}$ elastic scattering) to the OP was included in the calculations. The cross sections were calculated by numerical integration of the Schrödinger equation by means of the DWUCK4 code using all interactions obtained (Coulomb plus nuclear optical potential).

ii) The only free parameters in the hybrid model obtained by a fitting procedure to the experimental data whenever they exist are the coefficients N that correct the depths of the ReOP, ImOP, SO and surface potentials. These parameters (the deviations of their values from unity) can serve as a quantitative test of our method, but not as a tool to obtain a best agree-

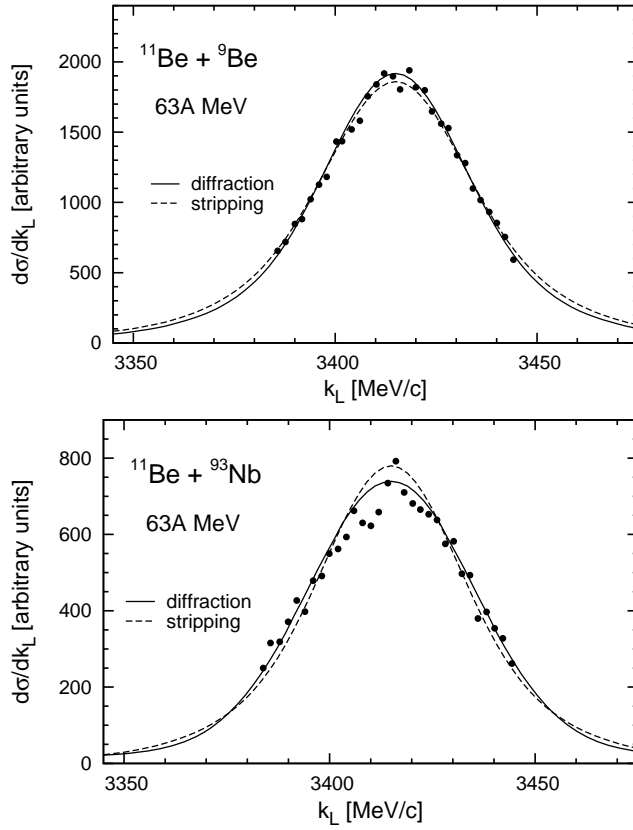


Figure 5: Cross sections of diffraction breakup and stripping reaction in $^{11}\text{Be}+^9\text{Be}$ and $^{11}\text{Be}+^{93}\text{Nb}$ scattering at $E = 63$ MeV/nucleon. Experimental data are taken from Ref. [26].

ment with the experimental data. A physical criteria imposed in our work on the choice of the values of the parameters N were the known behavior of the volume integrals J_V and J_W as functions of the incident energy in the interval $0 < E_{inc} < 100$ MeV/nucleon, as well as the values of the total cross section of scattering and reaction, if they are available.

iii) Other folding approaches are used to consider ^{11}Li breakup, suggesting a simple $^9\text{Li}+2n$ cluster model, and ^{11}Be breakup by means of the simple $^{10}\text{Be}+n$ cluster model. The latter models are applied to calculate the diffraction breakup and stripping reaction cross sections. It turns out that the breakup channel of $^{11}\text{Li}+p$ elastic scattering gives a breakup cross section that exceeds 80% of of the total reaction cross section, while it is about a half of the latter in the case of $^6\text{He}+^{12}\text{C}$ [30].

iv) Predictions for the longitudinal momentum distributions of ^9Li fragments produced in the breakup of ^{11}Li at 62 MeV/nucleon on a proton target are given. The widths of the peak we obtained are between 70 and 80 MeV/c, while widths of about 50 MeV/c are known from the reactions of ^{11}Li on nuclear targets ^9Be , ^{93}Nb , and ^{181}Ta at an energy of 66 MeV/nucleon.

v) The momentum distributions of ^{10}Be fragments produced in the breakup of ^{11}Be on ^9Be , ^{93}Nb , ^{181}Ta , and ^{238}U at 63 MeV/nucleon are obtained. There exists a good agreement of our calculations for the diffraction and stripping reaction cross sections with the available experimental data. The obtained widths of about 50 MeV/c are close to the empirical ones.

Concluding, we would like to note that future measurements of elastic scattering and breakup reactions of ^{11}Li , $^{10,11}\text{Be}$, and ^8B nuclei on different targets are highly desirable for the studies of the exotic nuclear structure. More complicated three-body approaches and more refined theoretical methods (e.g., CDCC method and its extensions) would allow an accurate interpretation of the expected data.

Acknowledgements

The authors are grateful to Professor N.S. Zelenskaya and Professor S.N. Ershov for helpful discussions and to Professor S.C. Pieper for providing with the density distributions of $^9,^{10}\text{Be}$ and $^7,^8\text{B}$ nuclei calculated within the QMC and VMS method, respectively. Four of the authors (D.N.K., A.N.A., M.K.G. and K.S.) are grateful for the support of the Bulgarian Science Fund under Contract No. DFNI-T02/19 and one of them (D.N.K.) under Contract No. DFNI-E02/6. The authors V.K.L., E.V.Z., and K.V.L. thank the Russian Foundation for Basic Research (Grant No. 13-01-00060) for partial support.

Bibliography

- [1] I. Tanihata, H. Hamagaki, O. Hashimoto, S. Nagamiya, Y. Shida, N. Yoshikawa, O. Yamakawa, K. Sugimoto, T. Kobayashi, D.E. Greiner, N. Takahashi, Y. Nojiri 1985 *Phys. Lett. B* **160** 380.
- [2] I. Tanihata, H. Hamagaki, O. Hashimoto, Y. Shida, N. Yoshikawa, K. Sugimoto, O. Yamakawa, T. Kobayashi, N. Takahashi 1985 *Phys. Rev. Lett.* **55** 2676.
- [3] V.K. Lukyanov, E.V. Zemlyanaya, K.V. Lukyanov, D.N. Kadrev, A.N. Antonov, M.K. Gaidarov, K. Spasova 2013 *Phys. Rev. C* **88** 034612.
- [4] V.K. Lukyanov, D.N. Kadrev, E.V. Zemlyanaya, K. Spasova, K.V. Lukyanov, A.N. Antonov, M.K. Gaidarov 2015 *Phys. Rev. C* **91** 034606.
- [5] K.V. Lukyanov, V.K. Lukyanov, E.V. Zemlyanaya, A.N. Antonov, M.K. Gaidarov 2007 *Eur. Phys. J. A* **33** 389.
- [6] V.K. Lukyanov, D.N. Kadrev, E.V. Zemlyanaya, A.N. Antonov, K.V. Lukyanov, M.K. Gaidarov 2010 *Phys. Rev. C* **82** 024604.
- [7] V.K. Lukyanov, E.V. Zemlyanaya, K.V. Lukyanov, D.N. Kadrev, A.N. Antonov, M.K. Gaidarov, S.E. Massen 2009 *Phys. Rev. C* **80** 024609.
- [8] K.V. Lukyanov, E.V. Zemlyanaya, V.K. Lukyanov 2006 *Phys. At. Nucl.* **69** 240; JINR Preprint P4-2004-115 2004 Dubna.
- [9] P. Shukla 2003 *Phys. Rev. C* **67** 054607.
- [10] D.T. Khoa, G.R. Satchler 2000 *Nucl. Phys. A* **668** 3.
- [11] R.J. Glauber (1959) in *Lectures in Theoretical Physics* (New York, Interscience) p.315.
- [12] A.G. Sitenko 1959 *Ukr. Fiz. J.* **4** 152.
- [13] S. Karataglidis, P.G. Hansen, B.A. Brown, K. Amos, P.J. Dortmans 1997 *Phys. Rev. Lett.* **79** 1447.
- [14] S. Karataglidis, P.J. Dortmans, K. Amos, C. Bennhold, *Phys. Rev. C* **61** 024319.
- [15] S.C. Pieper, K. Varga, R.B. Wiringa 2002 *Phys. Rev. C* **66** 044310.
- [16] P. Descouvemont 1997 *Nucl. Phys. A* **615** 261.
- [17] J. Carlson, S. Gandolfi, F. Pederiva, S.C. Pieper, R. Schiavilla, K.E. Schmidt, R.B. Wiringa 2015 *Rev. Mod. Phys.* **87** 1067.
- [18] K. Varga, Y. Suzuki, I. Tanihata 1995 *Phys. Rev. C* **52** 3013.
- [19] D.T. Khoa, W. von Oertzen 1993 *Phys. Lett. B* **304** 8; 1995 **342** 6; D.T. Khoa, W. von Oertzen, H.G. Bohlen 1994 *Phys. Rev. C* **49** 1652; D.T. Khoa, W. von Oertzen, A.A. Ogloblin 1996 *Nucl. Phys. A* **602** 98; D.T. Khoa, H.S. Than 2005 *Phys. Rev. C* **71** 014601; O.M. Knyaz'kov 1986 *Sov. J. Part. Nucl.* **17** 137.
- [20] P.D. Kunz, E. Rost, in *Computational Nuclear Physics* 1993 edited by K. Langanke et al., Vol. 2 (Springer-Verlag, New York), p.88.
- [21] C.-B. Moon et al. 1992 *Phys. Lett. B* **297** 39.
- [22] E.A. Romanovsky et al. 1998 *Bulletin of the Russian Academy of Sciences: Physics* **62** 150.
- [23] V. Lapoux et al. 2008 *Phys. Lett. B* **658** 198.
- [24] M.D. Cortina-Gil et al. 1997 *Phys. Lett. B* **401** 9; 1997 *Nucl. Phys. A* **616** 215c.
- [25] E.F. Aguilera et al. 2009 *Phys. Rev. C* **79** 021601(R).

Microscopic Optical Potential Description of Elastic Scattering ...

- [26] J.H. Kelley *et al.* 1995 *Phys. Rev. Lett.* **74** 30.
- [27] J.D. Patterson, R.J. Peterson 2003 *Nucl. Phys. A* **717** 235.
- [28] N.A. Orr *et al.* 1992 *Phys. Rev. Lett.* **69** 2050.
- [29] N.A. Orr *et al.* 1995 *Phys. Rev. C* **51** 3116.
- [30] V.K. Lukyanov, E.V. Zemlyanaya, K.V. Lukyanov 2011 *Int. J. Mod. Phys. E* **20** 2039.